DOI: 10.13009/EUCASS2017-218

Studies on Three-Dimensional Intake with Bleed at M_∞= 3.5

Manisankar Chidambaranathan and S B Verma***
**Senior Scientist*
Experimental Aerodynamics Division, CSIR-NAL, Bangalore, India
***Principal Scientist*
Experimental Aerodynamic Division. CSIR-NAL, Bangalore, India

Abstract
Experimental studies were carried out to understand the aerodynamic performance of a three dimensional sidewall inlet with the presence of bleed at M_∞= 3.5. The objective of the current work was to improve the inlet aerodynamic performance by having i) different sweep angles in both forward and reverse directions, ii) cowl extension iii) bleed. The result showed there is an optimum cowl length for which inlet performance is maximum. By having the bleed at the inlet entry the total pressure in the diffuser exhibit more uniformity across the section without major change in mass flow captured value of the inlet.

1. Introduction

For developing future hypersonic space transportation, air-breathing propulsion using scramjet engine is one of the key technology [1, 2]. The inlet particularly is of great importance for the optimal operation of the propulsion system. The efficient design of inlet depends on the amount of mass flow captured and the level of pressure recovery achieved before the combustion process. For achieving this goal, traditionally two dimensional inlet configuration as in figure. 1a is widely utilized. The major problem in using such two dimensional inlet configuration is its inability in handling different flow field condition as the vehicle accelerate/decelerate due to shock wave boundary layer interaction forming separation bubble as in figure. 1a leading to unstart phenomena [3]. On the other hand the three dimensional inlet [4] as in figure. 1b provides stable operation irrespective of the vehicle speed, through the spillage of mass prior to the inlet entry. In three dimensional inlets the flow is compressed in the horizontal direction using wedge shaped sidewalls. Whereas in the two dimensional inlets the flow is compressed in vertical direction which in turn induce more in plane turning of the flow leading to massive flow separation at the inlet entry [5,6].

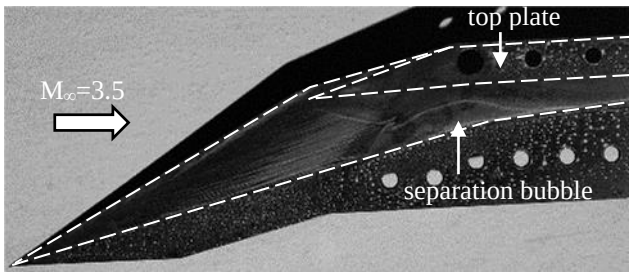

Figure. 1a Two dimensional inlet [6]

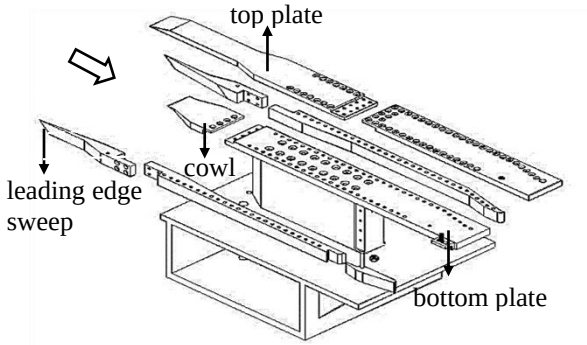

Figure. 1b Exploded view of three dimensional inlet

One of the major problem in the three dimensional inlets is its localized peak heating (ten times larger than two dimensional inlets [7]) at the corners due to the complex three dimensional interaction between the shock wave and the growing boundary layer. In addition to the above, the shock wave boundary layer interaction due to cowl extension of the inlet adds to the complexities. Stainback in 1960 [8] categorized the phenomena responsible for the increased heat transfer and skin friction in a three dimensional corner interaction as due to i) the vortex system produced from the leading edge of the corner ii) the reattachment followed by the shock-induced by the interaction. Much of the early works on three dimensional inlets were performed by Trexlar [9-13], to understand the aerodynamic performance of three dimensional inlets in detail. More detailed computational studies on three

DOI: 10.13009/EUCASS2017-218

dimensional inlets at lower supersonic Mach number were done by Kumar [14-15] which identified the advantage of having reverse sweep and improvement in scramjet inlet performance.

The objective of the current study is to improve the aerodynamic performance of the inlet through, i) the effect of leading edge sweep ($\alpha = 0°, 30°, 45°$) in both forward and reverse direction (ii) to study the effect of variation in the cowl extension length (Lcowl = 0h, 0.42h, 1.04h, 1.42h and 1.86h where h =24mm height of the isolator) (iii) to understand the effectiveness of bleed on controlling the corner effects in the inlet entry.

2. Experimental procedure and model setup

2.1 Wind tunnel facility details and test conditions

The experiments were conducted at CSIR-National Aerospace Laboratories (NAL), India. The tests were carried out at the 0.46 × 0.3 m trisonic blow down type wind tunnel at NAL. The wind tunnel operation is of intermittent and blow down type having capability to generate Mach number in the range of 0.3 to 4.0. The air is compressed at pressure of 10 bar and stored in 2800m^3 receiver which is discharged to the required test conditions using a Pressure Regulating Valve (PRV) which has a feedback control using NI based system. To provide optical access to the model being tested part of the test section wall is made up of glass window. The freestream Mach number was 3.5 ± 0.02, while the stagnation pressure P_o and temperature T_o were 682.58 kPa ± 2% (absolute) and 298 K ± 0.4%, respectively. The unit Reynolds number is 38.1×10^6 m^{-1}. The temperature at the wall is adiabatic approximately.

2.2 Model details

The inlet model is made up of modular construction with removable side wall sweep configurations ($\alpha = 0°, 30°, 45°$), different cowl lengths (L_{cowl} = 0h, 0.42h, 1.04h, 1.42h, and 1.86h where h =24mm height of the isolator) and a top wall as in figure.3. The model has an entry section of 48mm (w) × 24mm (h), followed by a converging section of 6 degree angle on both the sidewalls leading to a contraction ratio of 2.29. The leading edge sweep was maintained at sweep (both walls): 0˚; Forward (both walls): 30˚, 45˚; backward (both walls): 30˚, 45˚. The contraction region is followed by a constant area section also known as isolator with a length of 120 mm (5h) and 21mm (w). The combustion chamber in the inlet is simulated using a diffuser section after the isolator with a divergence angle of five degree, and length of 100 mm (4.17h). The model is elevated to the tunnel centreline using strut to avoid the interference from the tunnel wall boundary layer. The sidewall sweep was initially kept as zero on both the walls and the pressure measurements were carried out.

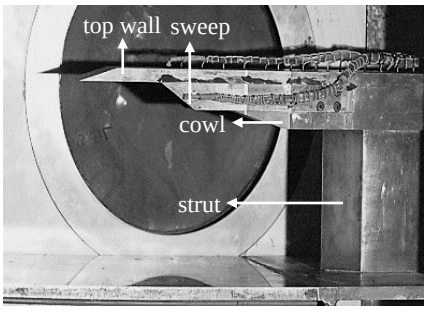

a) Model mounted inside the tunnel

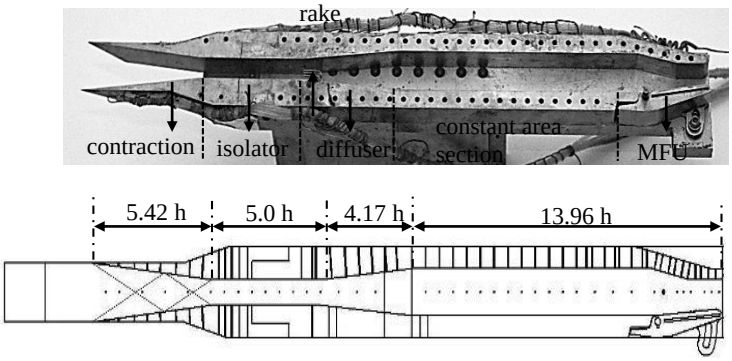

b) Model details

Figure. 2 Experimental setup and model view

Method suggested by Smart and Trexler [16] was used for measuring the mass flow through the inlet. The geometry is based on the deceleration of supersonic flow to lower Mach number through a shock wave and accelerating the subsonic flow to sonic condition through variable convergent area. The mass flow through the duct was measured using static pressure at two points near the exit of flap. Using the static pressure data at sonic point x/h = 32 and total pressure data at the point where the flow is subsonic x/h = 30, the Mach number M_3 is calculated. Mass flow is determined using the following formula

DOI: 10.13009/EUCASS2017-218

$$\mathrm{MFC} = \frac{(\rho_3 A_3 V_3 C_d)}{(\rho_1 A_1 V_1)}$$

Where ρ is density, A is the area, V is velocity and C_d is coefficient of discharge (0.9 for current study). The subscript 1 in the above formula denotes the freestream conditions and 3 denotes condition at sonic region inside the inlet. A six tube rake was located at the exit of the isolator (10.42h), to find the pressure recovery of the flow.

3. Results and Discussion

3.1 Effect of Cowl Length

Figure. 3a shows the mean wall pressure ratio distribution along the sidewall of the inlet for 0° sweep with different cowl lengths. As the cowl length was increased by1.86h relative to the baseline case there is an increase of pressure level in the contraction section (*x/h <10*) which may be attributed to the spillage shock formed ahead of the cowl leading edge. As the flow approaches the isolator region (*14 < x/h >10*) the pressure level was maintained almost constant value indicating the presence of separation bubble. Further downstream inside the diffuser there is a drastic rise in the pressure value which may be due to the presence of terminal shock in that region. As the flow passes through the constant area section (*x/h > 17*) it is further decelerated and becomes almost subsonic at *x/h > 26*. Inside the mass flow measurement unit (*x/h > 30*) the pressure value is decreased indicating the flow acceleration. Figure. 3b shows the centreline pressure distribution acquired along the top wall of the inlet model. The centreline pressure distribution at the contraction section(*x/h <10*) shows large increase in pressure as the cowl length extension is increased to 1.86h. At the beginning of the isolator region (*x/h=10*) there is a larger increase in the pressure value relative to the sidewall, which may be due to the fact that centreline experience multiple shock crossing from both the sidewall which is in addition to the cowl lip shock.

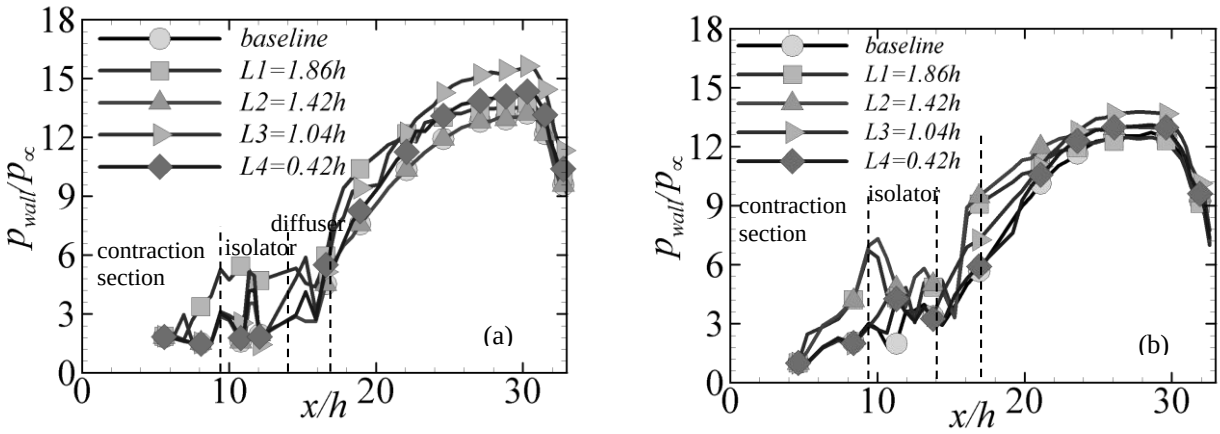

Figure. 3 Mean wall pressure distribution for cowl length extension along a) the sidewall b) the top wall

Figure. 4 shows the variation in mass flow captured (*MFC*) by the inlet for different cowl extension length (*L*) at zero degree sweep angle. It is evident that for the increase in the *L* with respect to the baseline case (where the cowl leading edge is at the isolator entry) *MFC* value improved. It is also observed that peak in *MFC* occurs for *L3=1.04h*, which is about 14% increase in *MFC* relative to the baseline case. Beyond the cowl extension of *L3* any further increase in the cowl extension length (*L2, L1*) seems to have only marginal rise in *MFC* of 6.5% and 5% relative to the baseline.

In-order to understand the reason behind the surge in the *MFC* at higher *L*, oil flow visualisation as in figure.5a-d was carried out for all the four cowl extension lengths, with zero degree leading edge sweep angle. Figure. 5a shows the oil flow visualisation for the *L1=1.86h*, the image clearly shows the presence of two separation bubble formed on either side of the sidewalls of the inlet. The presence of these separation bubbles indicate a strong interaction occurring between the cowl shock and the growing sidewall boundary layer of the inlet. Further on close observation of figure. 5a show traces of spillage shock formed ahead of the cowl lip. These spillage shock may be formed as a

DOI: 10.13009/EUCASS2017-218

result of the extension of cowl length. The reduction in the mass spillage due to extension of the cowl length adds to the mass flow entering the inlet, as the inlet cannot handle the additional mass leading to formation of the spillage

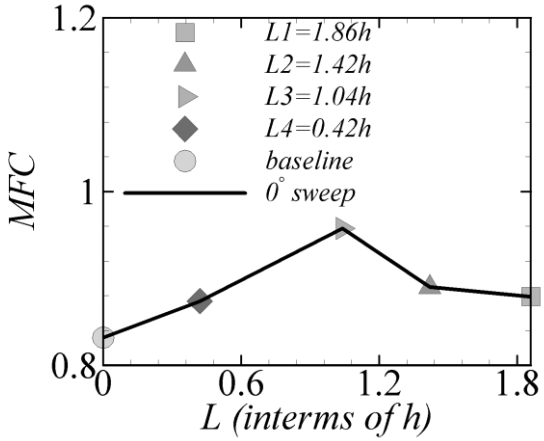

Figure. 4 variation in the mass flow captured (MFC) with cowl length extension

shock. When the cowl length extension was reduced to *L2* the separation bubble showed increase in width inside the inlet, added to that the spillage shock appears weaker as in figure. 5b. The spillage shock trace in the oilflow almost disappeared for the rest of the cowl lengths as seen in figure. (5c-5d). To summarise above discussion, as the cowl extension length is increased there is a reduction in the separation bubble width which adds to *MFC* leading to formation of spillage shock if the inlet mass handling capacity is exceeded . The above situation gives a clear indication there exist an optimum cowl length (in the current study *L3*) which has negligible spillage shock strength with moderate separation bubble width which possess larger *MFC* as discussed earlier.

Figure. 6a shows the total pressure profile at the entry to diffuser ($x/h=14$) along the span-wise direction for different cowl extension length with zero degree leading edge sweep. While approaching the centreline ($z/h=0.5$) of the inlet the plot shows the total pressure value tend to reach the maximum value. On the other hand total pressure value is at the least value closer to the sidewall, which is expected as the oil flow visualisation clearly showed presence of two separation bubble along the sidewall. The comparison of total pressure distribution between the baseline and cowl length extension of *L1*and *L3* shows that the increase in the cowl extension length has significant drop in the centreline total pressure value. The reason behind the larger drop in the centreline total pressure value with cowl length extension may be due to the combined effect of formation of spillage shock and presence of larger separation bubble. Figure. 6a shows that for the optimal cowl length extension (*L3*) the peak value of the total pressure ratio (P_o/P_∞) deviates from the baseline by almost -10.5% whereas for *L1* it was about -24% which indicates that the role of spillage shock associated loss has significant effect on the overall pressure recovery of the inlet.

Figure. 6b shows the maximum total pressure ratio ($P_{o,max}/P_\infty$) for different cowl length variation with zero degree leading edge sweep angle. The plot shows for the increase in cowl length extension the $P_{o,max}/P_\infty$, tend to reduce at lower cowl length extension (*L4*), about -3% relative to baseline. Whereas for *L3* it is -10.5% and for *L2* and *L1* it is about -16% and -24%. Although the cowl length extension is only increased at constant steps size of 0.4h, the loss in total pressure is non-linear which may be due to the fact that the total loss depends on the combined effect of both spillage shock and separation bubble width which varies depending on the cowl extension length.

DOI: 10.13009/EUCASS2017-218

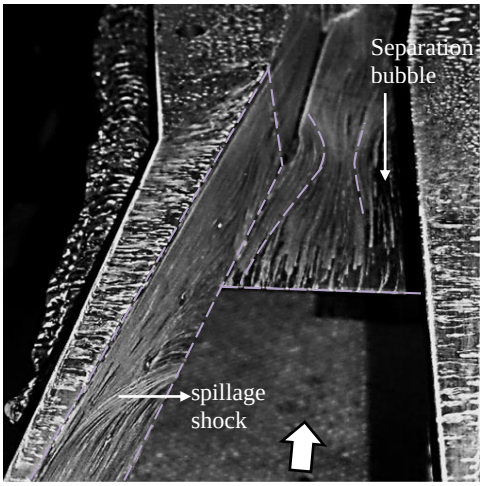

a) L1=1.86h

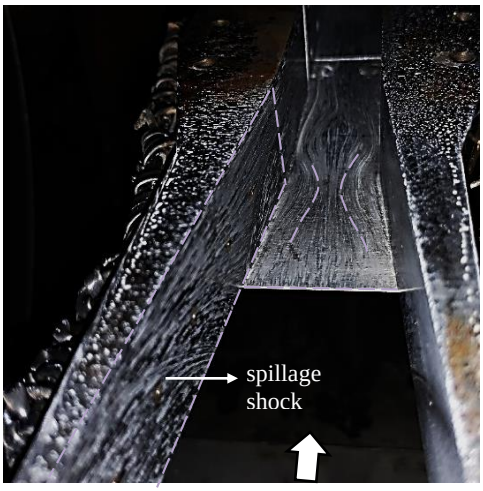

b) L2=1.42h

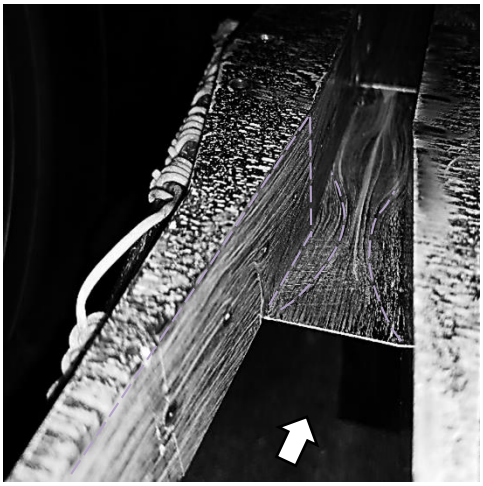

c) L3=1.04h

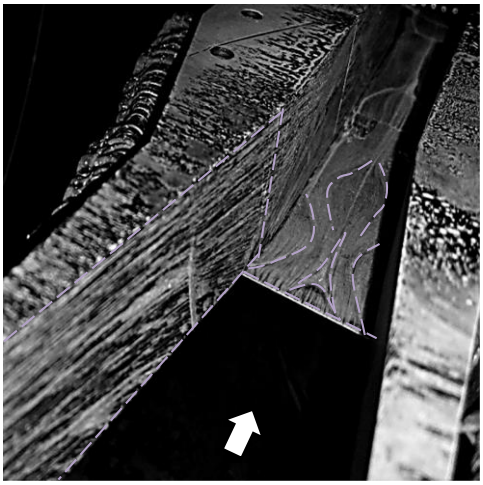

d) L4 =0.42h

Figure. 5 Oil flow visualisation for different cowl length extension

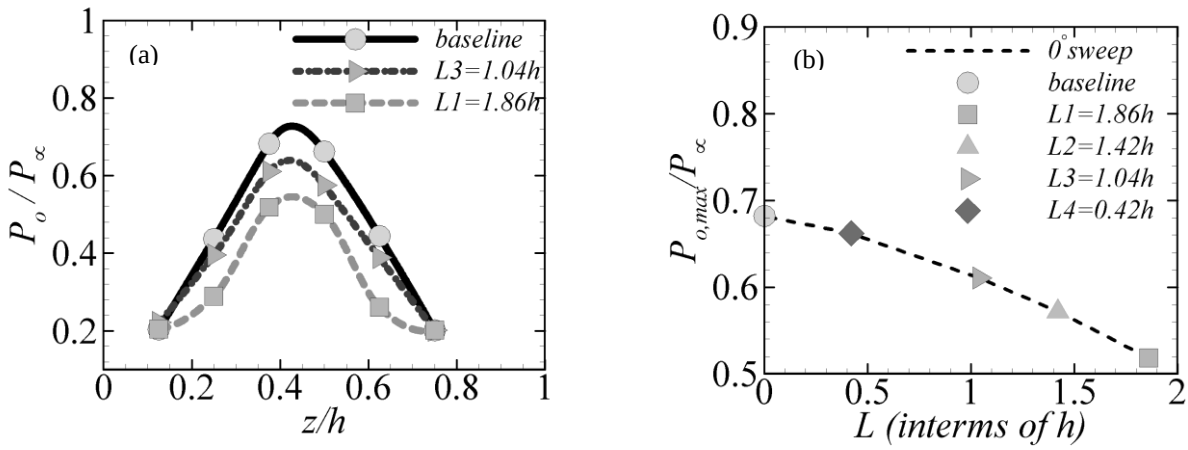

Figure. 6 total pressure variation a) along span-wise direction b) for various cowl length extension

DOI: 10.13009/EUCASS2017-218

3.2 Effect of leading edge sweep

Figure. 7a shows the sidewall pressure distribution with leading edge sweep variation of 0°, 30° and 45° in both forward (F) and backward (B) direction for the cowl extension length of *L1=1.86h*. When the sweep is in forward direction for both 30° and 45° the pressure rise associated with the spillage shock in the contraction section shows some modifications. There is a larger shift in stream wise direction pressure rise for 30°F, which may be due to the effect of change in the mean flow orientation towards the inlet by the forward sweep, resulting in more mass trying to enter the inlet than it can actually handle which in-turn strengthen the spillage shock. The effect of sweeping the leading edge in backward direction doesn't seems to have major impact on the sidewall pressure distribution for both 30° and 45°, where it almost overlap with the baseline case. Figure. 7b also shows the top wall pressure distribution for sweep angle of 0°, 30° and 45° in both forward (F) and backward (B) direction for the cowl extension length of *L1=1.86h*. The top wall also show increased pressure value for the 30° forward sweep in the isolator region, however there is a minimal variation for the backward sweep case for all the sweep angles.

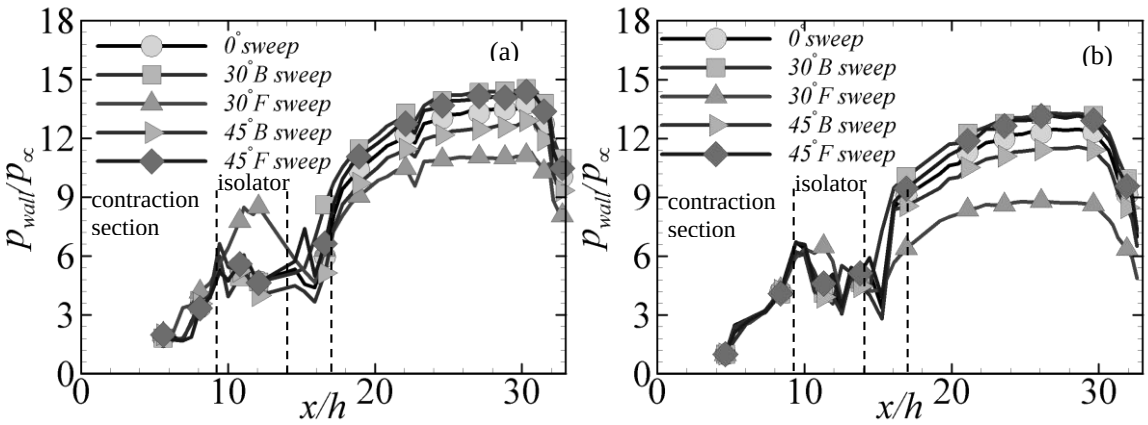

Figure. 7 Mean wall pressure distribution for different sweep leading edge angle along a) the sidewall b) the top wall

Figure. 8a-8b shows the *MFC* for the inlet with leading edge sweep of 0°, 30° and 45° in both forward (F) and backward (B) direction for the variation in the cowl extension length (*L*). As the *L* is increased all the sweep angles showed an increase in the *MFC* of the inlet till the optimum cowl length *L3* as discussed earlier in subsection 3.1. The base line case in the plot shows by having a sweep of 30° in forward direction the *MFC* increases to about 15% relative to the 0° sweep case. At the same instance by having the sweep of 30° in backward direction the *MFC* reduced by -9.5%. For *L4* the variation in the *MFC* is almost same as that of the baseline case with peak in *MFC* is observed for the 30° forward case. However for the *L3* case the difference in *MFC* between 0°, 30°F was about 4% higher than 0° whereas -9% lesser for the 30°B. When the cowl length extension is increased to *L2* the 30°F case shows opposite trend to that of *L3* with -8.4% reduction in *MFC* relative to the 0°, on the other hand it shows 5.6% increase in *MFC* for the 30°B case.

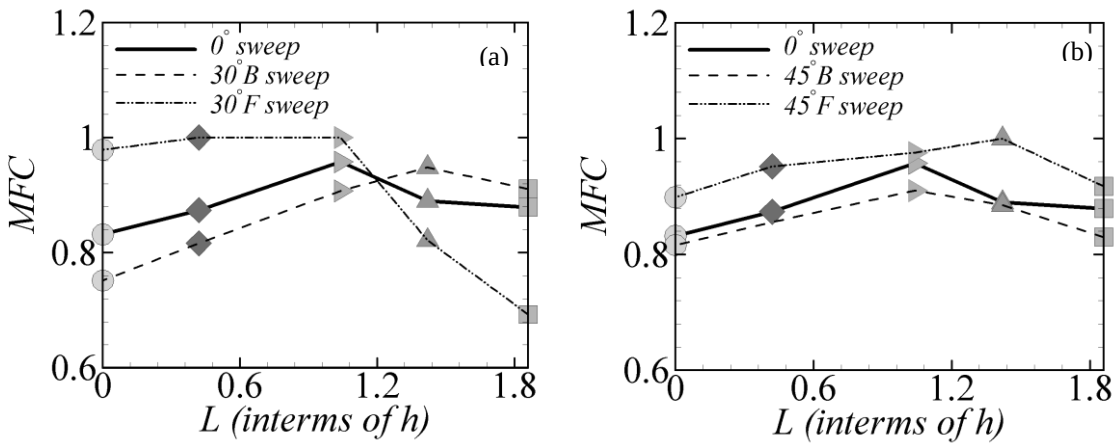

Figure. 8 *MFC* variation a) for 30° sweep variation b) 45° sweep variation

DOI: 10.13009/EUCASS2017-218

In the case of the larger cowl length extension *L1* the 30°F continue to have reduction in *MFC* of -27.5% relative to the 0° sweep. The sudden drop in *MFC* level for the forward sweep may be attributed to the formation of the spillage shock ahead of the cowl lip. For the baseline case at 45°F sweep there is about 6% increase in *MFC* relative to 0° sweep. The reduction in the *MFC* as the sweep angle is changed in forward direction (15% for 30°F; 6% for 45°F) signifies the role of leading edge sweep in modifying the inlet flow conditions. In-case of *L2* for the 45°F sweep *MFC* increase by 12% (whereas for 30° F it was -8.4%) which emphasis by changing the sweep angle the formation of the spillage shock can be delayed. For the larger cowl length *L1* the 45° forward sweep is able to have relatively better *MFC* of about 4% (for 30° F it was -27.5%) which clearly shows by controlling the spillage shock strength it is possible to achieve better *MFC* by the inlet.

Figure. 9 shows the maximum total pressure recovery across the span wise distribution for the sidewall leading edge sweep of 0°, 30° and 45° in both forward (F) and backward (B) direction with cowl length extension of *L1=1.86h*. It is evident from the plot that there is no major change in the maximum total pressure ratio ($P_{o,\,max}/P_{\infty}$) value between the backward and 0° sweep, which is expected as the *MFC* shows no major change in its value between the 0° and backward sweep case. However in the case of 30°F the $P_{o,\,max}/P_{\infty}$ shows a drop of about 12.5% in value which may be the result of increase of the spillage shock strength as discussed earlier.

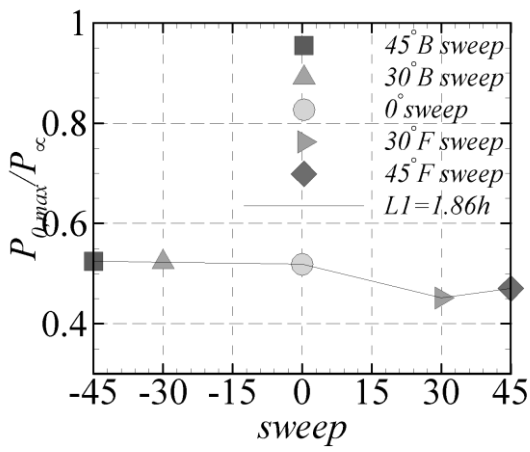

Figure. 9 Total pressure variation with different sweep angles

3.3 Effect of bleeding

Figure. 10a shows the schlieren flow visualisation without bleed for the 30°F sweep having *L1=1.86h*. It is clear from the picture that the spillage shock is formed ahead of the cowl lip in the contraction section. As the inlet model is made of metal surface the internal flow couldn't be visualised properly. Figure .10b shows the schlieren image with bleed of $Y_{bleed} = 0.067h$ for the 30°F sweep having *L1=1.86h*. The image shows by having the bleed the spillage shock disappears, which may be due to the reduction of separation bubble inside the sidewall as discussed earlier in the sub-section 3.1.

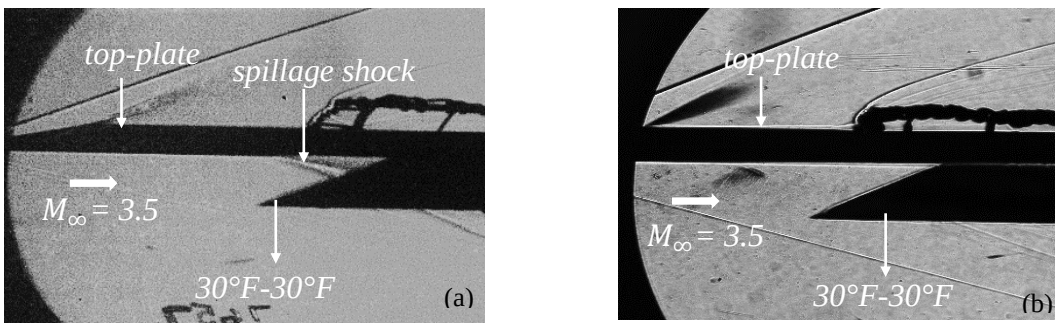

Figure. 10 Schlieren flow visualisation a) without bleed b) with bleed Y_{bleed}=0.067h

DOI: 10.13009/EUCASS2017-218

Figure. 11 shows the *MFC* with different sweep angles for *L1=1.86h* without and with bleed of $Y_{bleed}=0.067h$. The effect of introducing bleed seems to reduce the *MFC* for 45°B by -8.4% and for 30°B by 8.8% relative to no-bleed case. For 0° case with and without bleed values have minimal deviation in the *MFC* value. The effect having bleed seems to more helpful when the sweep is at forward as in the case of 30°F almost 8% increase in the *MFC*.

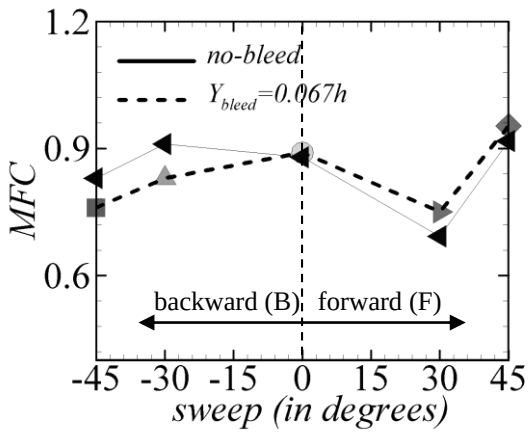

Figure. 11 Variation in *MFC* for different sweep angles with and without bleed

Figure. 12 shows the total pressure ratio P_o/P_∞ along the span wise direction with and without bleed for different sweep angles. With the introduction of the bleed, almost for all the sweep angles the total pressure ratio profile shows more uniform distribution along the span wise direction. The recovery of the total pressure along the sidewall may be due to the reduction in the sidewall separation bubble width as the bleed helps to remove the adverse pressure gradient formed due to the interaction between the cowl lip shock and the sidewall boundary layer.

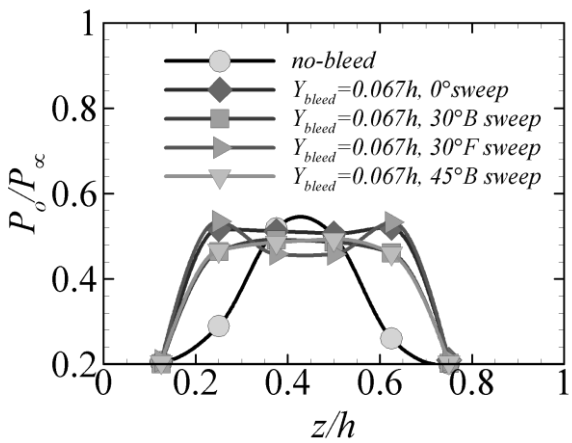

Figure. 11 Variation in total pressure along span-wise direction for different sweep angles with and without bleed

4. Conclusion

Experimental studies were carried out at M_∞=3.5 to understand the aerodynamic characteristic of a three dimensional inlet with and without bleed. The effect of increasing the cowl length was studied with five different cowl lengths relative to the baseline case. The leading edge sweep angle was varied between 0°, 30° and 45° and tested for all the cowl lengths. The model is made of modular construction consisting of inlet unit and a mass flow measurement unit. The mean wall pressure values were obtained on both sidewalls and the top wall of the model. In addition to the wall pressure measurement total pressure profile was obtained at the inlet of the diffuser section for all the cowl length variation and sweep angles. The result shows there exist an optimum cowl length *L3* for which the *MFC* improves and reaches a peak value of about 14% with 0° sweep angle. Any further increase in cowl length beyond the optimal

cowl length extension (*L3*) shows reduction of *MFC*. The oil flow visualisation for the cowl length variation showed the traces of spillage shock as the cowl length extension crosses *L3*. The oil flow further revealed the presence of strong separation bubble located closer to the side walls of the inlet. The total pressure profile shows a drop in value nearer to the wall surface reiterating the presence of strong separation bubble near to sidewall region. The maximum value for the total pressure value seems to reduce as the cowl length is increased which may be due to combined loss caused by spillage shock and separation bubble. The 45° sweep angle showed better *MFC* relative to the 30° case for all the cowl length extensions. Among the forward and backward sweep combinations the forward case shows larger *MFC* for all the cowl length extension. On the other hand the backward sweep performed better in terms of pressure recovery value relative to the zero degree sweep angle.

The introduction of bleed $Y_{bleed} = 0.067h$ resulted in the improvement of the *MFC* for the forward sweep case. The schlieren flow visualisation with the bleed showed absence of the spillage shock for the cowl length extension of 1.86h. The total pressure profile became more uniform with the introduction of the bleed reiterating the fact with the introduction of the bleed the width of the separation bubble is reduced resulting in larger total pressure recovery.

References

[1] P.L.Moses,K A Bouchard,R F Vause S Z Pinckney: An Air breathing launch vehicle design with turbine based low speed propulsion and dual mode scram jet high speed propulsion: *9th International Space Planes and Hypersonic Systems and Technologies Conference*, November 1-5, 1999, AIAA Paper No. 99-4948.

[2] Francois Falempin, Laurent Serre: *12th AIAA International Space planes and Hypersonic systems and Technologies*, 15 – 19, December 2003, AIAA 2003 – 7031.

[3] D. Van Wie, F. Kwok, and R. Walsh: Starting characteristics of supersonic inlets, *32nd Joint Propulsion Conference and Exhibit, Joint Propulsion Conference*, July, 1996, AIAA Paper No. 96-2914.

[4] Holland, Scott Perkins, Jhon: Internal shock interactions in propulsion/airframe integrated three-dimensional sidewall compression scramjet inlets, *28th Joint Propulsion Conference and Exhibit*, 1992, AIAA Paper No. 92-3099.

[5] Holland, S. D., and Perkins, J. N.(1990): Mach 6 Testing of Two Generic Three-Dimensional Sidewall Compression Scramjet Inlets in Tetrafluoromethane, *AIAA 28th Aerospace Sciences Meeting*, January 8-11,1990, Reno, NV, AIAA-90-0530.

[6] C. Manisankar,and Sajeer, Ahmed and Thiagarajan, V : Investigation of starting process of a movable intake configuration at high supersonic speeds, *Proceedings of the 13th Asian Congress of Fluid Mechanics*, 17-21 Dec 2010, Dhaka, Bangladesh.

[7] Holland, S.D., : A Computational and Experimental Investigation of a Three-Dimensional Hypersonic Scramjet Inlet Flow Field, Ph.D Thesis, Raleigh, North Carolina, 1991

[8] Stainback, P. Calvin: An Experimental Investigation at a Mach Number of 4.95 of Flow in the Vicinity of a 90 deg Interior Comer Alined with theFree-Stream Velocity, *NASA TN D-184*, Feb. 1960.

[9] Trexler, Carl A.: Performance of an Inlet for an Integrated Scramjet Concept. *J. Aircraft*, Vol. 11, No.9, September 1974.

[10] Trexler, Carl A.: Inlet Performance of the Integrated Langley Scramjet Module (Mach 2.3 to 7.6), *AIANSAE 11th Propulsion Conference*, Sept.29-0ct.1, 1975, Anaheim, CA, AIAA-75-1212.

[11] Trexler, Carl A: Tests of Two Sidewall-Compression Scramjet Inlets at Mach 18.1 to 21.6 in Helium, *National Aero-Space Plane Technology Report*, February, 1988.

[12] Trexler, Carl A., and Souders, Sue W.: Design and Performance at a Local Mach Number of 6 of an Inlet for an Integrated Scramjet Concept. *NASA TN D-7944*, August 1975.

[13] Trexler, Carl A: Inlet Starting Predictions for Sidewall-Compression Scramjet Inlets, *AIAA/SAE/ASME/ASEE 24th Joint Propulsion Conference*, July 11-13, 1988, Boston, AIAA-88-3257.

[14] Kumar, A.: Three-Dimensional Inviscid Analysis of the Scramjet Inlet Flow Field, *AIAA 20th Aerospace Sciences Meeting*, Orlando, Jan. 11-14, 982. AIAA-82-0060.

[15] Kumar, Ajay, Singh, D. J., and Trexler, C. A.(1990): A Numerical Study of the Effects of Reverse Sweep on a Scramjet Inlet Performance. Presented at the AIANSAE/ASME/ASEE *26th Joint Propulsion Conference*, Orlando, July 16-18, 1990, AIAA-90-2218.

[16] Michael K Smart and Carl A Trexler.: Mach 4 performance of hypersonic inlet with rectangular to elliptical shape transition, *Journal of Propulsion and Power*, Vol. 20, No.2, March – April 2004, P 288 – 293.